Convective Boundary Layers Driven by Nonstationary Surface Heat Fluxes

ROBERT VAN DRIEL AND HARM J. J. JONKER

Department of Multi-Scale Physics, Delft University of Technology, Delft, Netherlands

(Manuscript received 12 August 2010, in final form 17 November 2010)

ABSTRACT

In this study the response of dry convective boundary layers to nonstationary surface heat fluxes is systematically investigated. This is relevant not only during sunset and sunrise but also, for example, when clouds modulate incoming solar radiation. Because the time scale of the associated change in surface heat fluxes may differ from case to case, the authors consider the generic situation of oscillatory surface heat fluxes with different frequencies and amplitudes and study the response of the boundary layer in terms of transfer functions. To this end both a mixed layer model (MLM) and a large-eddy simulation (LES) model are used; the latter is used to evaluate the predictive quality of the mixed layer model. The mixed layer model performs generally quite well for slow changes in the surface heat flux and provides analytical understanding of the transfer characteristics of the boundary layer such as amplitude and phase lag. For rapidly changing surface fluxes (i.e., changes within a time frame comparable to the large eddy turnover time), it proves important to account for the time it takes for the information to travel from the surface to higher levels of the boundary layer such as the inversion zone. As a follow-up to a 1997 study by Sorbjan, who showed that the conventional convective velocity scale is inadequate as a scaling quantity during the decay phase, this paper addresses the issue of defining, in (generic) transitional situations, a velocity scale that is solely based on the surface heat flux and its history.

1. Introduction

Real planetary boundary layers (PBLs) are often in a state of transition, adapting to changing boundary conditions or large-scale forcings. Examples are sunset and sunrise, modulation of solar irradiance by clouds, and large-scale advection of air with different properties. Knowledge of the behavior of transitional atmospheric boundary layers is therefore as relevant as knowledge about their steady-state counterparts.

A number of observational and modeling studies have addressed the morning transition (e.g., Angevine et al. 2001; Lapworth 2006; Beare 2008) and the evening transition (e.g., Mahrt 1981; Acevedo and Fitzjarrald 2001; Lapworth 2003; Beare et al. 2006; Grant 1997). Apart from the early and late evening transitions, it is useful to also distinguish the so-called late afternoon transition (e.g., Pino et al. 2010; Sorbjan 2007) during which the surface heat flux is declining but is still nonnegative. This situation of decaying convective turbulence was studied by Nieuwstadt and Brost (1986) using a large-eddy simulation (LES) model. Treating the transition in a simple way by abruptly switching of the surface heat flux, they found the turbulence kinetic energy to decay according to a power law $k \sim t^{-n}$, with n close to 1.2. Pino et al. (2006) extended this work by studying the influence of wind shear during the convective decay. In addition they analyzed the characteristic length scales of the velocity fields during the decay and showed that the characteristic length scale of horizontal length scales significantly increases during the transition, as opposed to the typical length scale of the vertical velocity, which remains bounded by the boundary layer depth. The increasing length scales were shown to be responsible for the relatively slow decay already observed by Nieuwstadt and Brost (1986)—that is, the fact that the exponent n in the decay law $k \sim t^{-n}$ is close to 1 rather than 2, where the latter value is to be expected if the dominant length scales were confined to the PBL depth.

Instead of an abrupt change in the surface heat flux, Sorbjan (1997) considered the more common situation of a gradually decreasing surface flux following a cosine shape and pointed out that this has a pronounced impact

Corresponding author address: Harm Jonker, Dept. of Multi-Scale Physics, Delft University of Technology, P.O. Box 5046, 2600 GA, Delft, Netherlands.
E-mail: h.j.j.jonker@tudelft.nl

DOI: 10.1175/2010JAS3643.1

on the decay law and also that the convective velocity scale based on the actual surface flux was a poor predictor of the actual velocity variances and turbulence kinetic energy. This scaling issue has also been addressed in a study of observations during a full diurnal cycle (Kumar et al. 2006). In addition, there have been studies on the effects of a solar eclipse (Dolas et al. 2002; Girard-Ardhuin et al. 2003) and also the turbulence decay during an eclipse (Anfossi et al. 2004). A theoretical approach was conducted by Goulart et al. (2003).

The problem of scaling during the diurnal cycle and especially the sunset phase forms the motivation of this research. We focus on the response of a convective boundary layer to changes in the surface heat flux. This is relevant not only during sunrise and sunset but also when, for example, clouds disturb the incoming solar radiation. But because the time scale of the associated change in surface heat fluxes may differ from case to case—sunrise/sunset rate, for example, is latitude and season dependent, and modulation of sunlight by clouds can occur on a variety of time scales—we consider below the generic situation of oscillatory surface heat fluxes with different frequencies and amplitudes and study the response of the boundary layer characteristics, in particular PBL depth and inversion strength, in terms of transfer functions (amplitude and phase difference). We employ both a large-eddy simulation and a mixed layer model (MLM) (e.g., Tennekes 1973; Vilà-Guerau de Arellano et al. 2004); the LES is used to evaluate the predictive quality of the mixed layer model, whereas the mixed layer model helps to provide fundamental insight into the characteristics of the boundary layer system.

2. Case and model description

a. Case description

We consider a dry convective boundary layer in absence of mean wind and Coriolis force (e.g., Jonker et al. 1999). The free atmosphere is stably stratified with lapse rate Γ. Turbulence is driven by a positive surface heat flux ϕ_s, initially taken as constant ($=\phi_0$), which causes a well-mixed layer that deepens by entrainment. This growth is counteracted by the presence of subsidence w_s, which for simplicity is taken as constant with height, except for the lowest part of the PBL. To ensure a steady situation in the overlaying layer (free troposphere), we have also introduced a constant radiative cooling term R:

$$R = w_s \Gamma. \tag{1}$$

The profiles of (initial) potential temperature, subsidence and radiation are shown in Fig. 1. Other settings are listed in Table 1. The LES model employed here is the Dutch Atmospheric Large-Eddy Simulation (DALES) model described in detail in Heus et al. (2010).

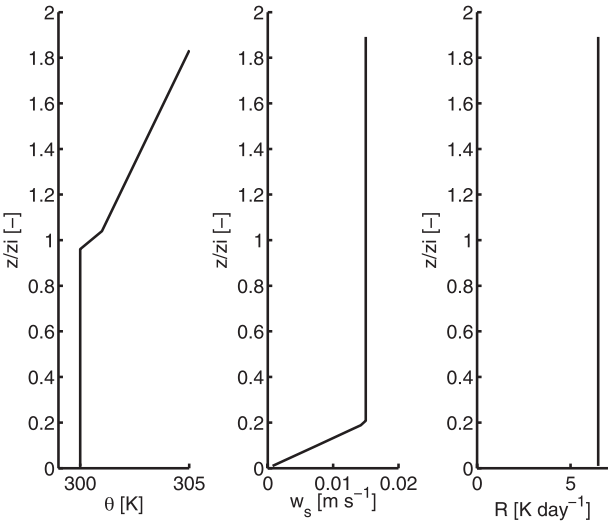

FIG. 1. Vertical profiles used in the LES: (left) initial potential temperature, (middle) subsidence, and (right) radiative cooling terms.

b. Mixed layer model for stationary fluxes

The graphical interpretation of the case within the context of a mixed layer model is shown in Fig. 2. Taking subsidence and radiative cooling into account, we arrive at the following equations for the mixed layer model:

$$\frac{\partial \theta}{\partial t} = \frac{\phi_s - \phi_e}{z_i} - R, \tag{2}$$

$$\frac{\partial \Delta}{\partial t} = \Gamma w_e - \frac{\partial \theta}{\partial t} - R, \quad \text{and} \tag{3}$$

$$\frac{\partial z_i}{\partial t} = w_e - w_s, \tag{4}$$

where ϕ_e is the entrainment flux, w_e is the entrainment velocity, and R is the radiative forcing in the mixed layer and the free atmosphere. Note our convention to define w_s as positive while incorporating it with a minus sign in Eq. (4) to account for the downward motion that it

TABLE 1. LES and MLM settings.

Domain size ($L_x \times L_y \times L_z$)	$5120 \times 5120 \times 1920$ m^3
Grid size ($d_x \times d_y \times d_z$)	$40 \times 40 \times 20$ m^3
No. of grid points	$128 \times 128 \times 96$
Lapse rate (Γ)	0.005 K m^{-1}
Subsidence (w_s)	0.015 m s^{-1}
Surface heat flux (steady; ϕ_0)	0.06 K m s^{-1}
Initial inversion height (z_{i0})	1000 m
Initial inversion strength (Δ_0)	1.0 K

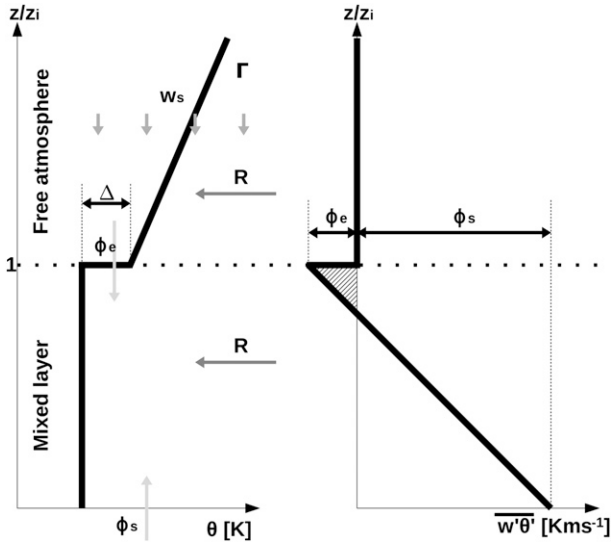

FIG. 2. The mixed layer model setup in this research: (left) the vertical profile of the potential temperature and (right) the vertical profile of the turbulent heat flux.

represents. The same convention is used for the radiative cooling tendency. Using a zero-order model (Lilly 1968), the entrainment flux can be expressed in terms of the entrainment velocity and inversion strength Δ:

$$\phi_e = -w_e\Delta. \tag{5}$$

To close the model, the entrainment flux is assumed to be a constant fraction of the surface flux (e.g., Ball 1960; Tennekes 1973):

$$\phi_e = -A\phi_s, \tag{6}$$

where A is the entrainment ratio with a typical value of 0.2–0.3. This results in a system governed by the following equations:

$$\frac{\partial\Delta}{\partial t} = \frac{A\phi_s\Gamma}{\Delta} - \frac{(1+A)\phi_s}{z_i} = f(\Delta, z_i, \phi_s) \quad \text{and} \tag{7}$$

$$\frac{\partial z_i}{\partial t} = \frac{A\phi_s}{\Delta} - w_s = g(\Delta, z_i, \phi_s). \tag{8}$$

c. *Fixed points and stability in the case of a stationary heat flux*

With a uniform (i.e., height independent) subsidence profile, it is a priori unclear whether in general a steady state can be reached. This question can be conveniently addressed by analyzing the mixed layer model equations (i.e., by finding the fixed points and classifying their stability). In addition, this provides information on the inherent time scales of the system. Assuming a stationary $\phi_s = \phi_0$, the fixed points of the system (7) and (8) can be determined by setting $\partial\Delta/\partial t = \partial z_i/\partial t = 0$. This results in only one fixed-point solution (Δ_0, z_{i0}):

$$\Delta_0 = \frac{A\phi_0}{w_s} \quad \text{and}$$
$$z_{i0} = \frac{(1+A)\phi_0}{\Gamma w_s}. \tag{9}$$

We note in passing that these values together with Eq. (1) imply also that $\partial\theta/\partial t = 0$.

The local stability of the fixed point can be studied by perturbing it slightly:

$$\Delta(t) = \Delta_0 + \Delta'(t) \quad \text{with} \quad \Delta' \ll \Delta_0, \quad \text{and}$$
$$z_i(t) = z_{i0} + z_i'(t) \quad \text{with} \quad z_i' \ll z_{i0}. \tag{10}$$

Neglecting higher-order terms of the perturbations, one arrives at the following form:

$$\frac{\partial}{\partial t}\begin{pmatrix}\Delta'\\ z_i'\end{pmatrix} = J(\Delta_0', z_{i0})\begin{pmatrix}\Delta'\\ z_i'\end{pmatrix}, \tag{11}$$

where J is the Jacobian

$$J = \begin{pmatrix}\dfrac{\partial f}{\partial\Delta} & \dfrac{\partial f}{\partial z_i}\\ \dfrac{\partial g}{\partial\Delta} & \dfrac{\partial g}{\partial z_i}\end{pmatrix} \tag{12}$$

and $J(\Delta_0, z_{i0})$ denotes the Jacobian in the fixed point, which is given by

$$J(\Delta_0, z_{i0}) = \begin{pmatrix}-\dfrac{w_s^2\Gamma}{A\phi_0} & \dfrac{\Gamma^2 w_s^2}{(1+A)\phi_0}\\ -\dfrac{w_s^2}{A\phi_0} & 0\end{pmatrix}. \tag{13}$$

The eigenvalues of the Jacobian, which reveal the stability of the fixed point, are found to be

$$\lambda_{1,2} = -\frac{1 \pm \sqrt{(1-3A)/(1+A)}}{2A}\frac{\Gamma w_s^2}{\phi_0}. \tag{14}$$

Clearly the real parts of the eigenvalues are always negative, which implies that the fixed point is unconditionally stable. The eigenvalues are complex valued when $A > \frac{1}{3}$, indicative of (damped) oscillatory behavior. The eigenvalues also give insight into the inherent time scales of the system. When $0 < A < \frac{1}{3}$ there

are two time scales given by the negative reciprocal value of the eigenvalues:

$$\tau_{\pm} = \frac{2A}{1 \pm \sqrt{(1-3A)/(1+A)}} \frac{\phi_0}{\Gamma w_s^2}. \tag{15}$$

When $\frac{1}{3} \leq A < 1$ the eigenvalues are complex valued and the response time scale follows from the real part:

$$\tau = \frac{2A\phi_0}{\Gamma w_s^2}. \tag{16}$$

d. Fixed points and stability in the case of a nonstationary heat flux

Similar calculations can be performed for the case of a nonstationary surface heat flux $\phi_s(t) = \phi_0 + \phi'(t)$ when we assume that amplitude of the fluctuations are small. The fixed point of the system is the same as in the case of a stationary flux (9), but the (linearized) perturbed system now reads

$$\frac{\partial}{\partial t}\begin{pmatrix} \Delta' \\ z_i' \end{pmatrix} = J(\Delta_0, z_{i0}, \phi_0)\begin{pmatrix} \Delta' \\ z_i' \end{pmatrix} + \begin{pmatrix} \dfrac{\partial f}{\partial \phi_s} \\ \dfrac{\partial g}{\partial \phi_s} \end{pmatrix}\phi', \tag{17}$$

where $J(\Delta_0, z_{i0}, \phi_0)$ is again the Jacobian in the fixed point. The driver of the system is ϕ'; Δ' and z_i' respond to this driver. Taking

$$\begin{aligned} \phi' &= \hat{\phi} e^{iwt}, \\ \Delta' &= \hat{\Delta} e^{iwt}, \\ z_i' &= \hat{z}_i e^{iwt}, \end{aligned} \tag{18}$$

the system (17) becomes

$$i\omega\begin{pmatrix} \hat{\Delta} \\ \hat{z}_i \end{pmatrix} = J(\Delta_0, z_{i0}, \phi_0)\begin{pmatrix} \hat{\Delta} \\ \hat{z}_i \end{pmatrix} + \begin{pmatrix} 0 \\ \dfrac{w_s}{\phi_0} \end{pmatrix}\hat{\phi}. \tag{19}$$

This can be written as

$$\begin{pmatrix} \hat{\Delta} \\ \hat{z}_i \end{pmatrix} = \{i\omega \mathbf{I} - J(\Delta_0, z_{i0}, \phi_0)\}^{-1} + \begin{pmatrix} 0 \\ \dfrac{w_s}{\phi_0} \end{pmatrix}\hat{\phi}, \tag{20}$$

where $\mathbf{I}$ is the unit matrix. Solving Eq. (20) gives the responses $\hat{\Delta}$ and $\hat{z}_i$ as a function of ω:

$$\hat{\Delta} = \frac{w_s^3 \Gamma^2 A \hat{\phi}}{\phi_0^2 \omega^2 A(1+A) - \Gamma^2 w_s^4 - i\phi_0 \omega \Gamma w_s^2 (1+A)} \quad \text{and} \tag{21}$$

$$\hat{z}_i = \frac{w_s(i\omega A\phi_0 + \Gamma w_s^2)(1+A)\hat{\phi}}{\phi_0^2 \omega^2 A(1+A) - \Gamma^2 w_s^4 - i\phi_0 \omega \Gamma w_s^2 (1+A)}. \tag{22}$$

Without loss of generality we can set $\hat{\phi} = 1$. Furthermore, it is convenient to express the response $\hat{z}_i$ in an amplitude $Z(\omega) = |\hat{z}_i|$ and phase difference $\Psi(\omega)$:

$$\hat{z}_i = Z(\omega) e^{i\Psi(\omega)}. \tag{23}$$

We emphasize that the above expressions for the response of the mixed layer to nonstationary fluxes are derived for very small fluctuations around the basic state. Since the original system is nonlinear, one cannot directly generalize this behavior for larger-amplitude variations. In the next section both the LES and the mixed layer model will be subjected to finite surface flux variations of the form

$$\phi_s(t) = \phi_0 + \alpha \sin(\omega t) = \phi_0 + \alpha \sin\left(\frac{2\pi}{T} t\right), \tag{24}$$

where α is the amplitude, ω is the frequency of the surface heat flux, T is the period of the surface heat flux, and ϕ_0 is the average surface heat flux; α will be taken as large as ϕ_0. The resulting response of the PBL will be compared to the predictions of the linearized response (22).

3. Results

a. LES and the standard mixed layer model

Figure 3 shows an example of a periodically oscillating heat flux using Eq. (24) with $\alpha = \phi_0$ and $T = 4$ h; below we have shown the evolution of z_i as simulated with the LES, where z_i was determined by locating the maximum gradient[1] in the mean profile of θ (Sullivan et al. 1998). One can notice a significant delay $t_L \simeq 1$ h between z_i and ϕ_s, which expressed in terms of Ψ reads

$$t_L = \frac{\Psi T}{2\pi}, \tag{25}$$

showing that the corresponding phase difference amounts to $\Psi \approx \pi/2$. We will study the phase lag as well as the amplitude of the response in more detail below, but first we show the mean profiles of the LES at different stages in Fig. 4. These are so-called phase-conditioned

[1] An alternative for determining z_i is to locate the height of the minimum buoyancy flux, but this method proved to be rather cumbersome for varying surface buoyancy fluxes, mainly because the buoyancy flux profiles no longer display the universal (linear) shape (e.g., Sorbjan 1997).

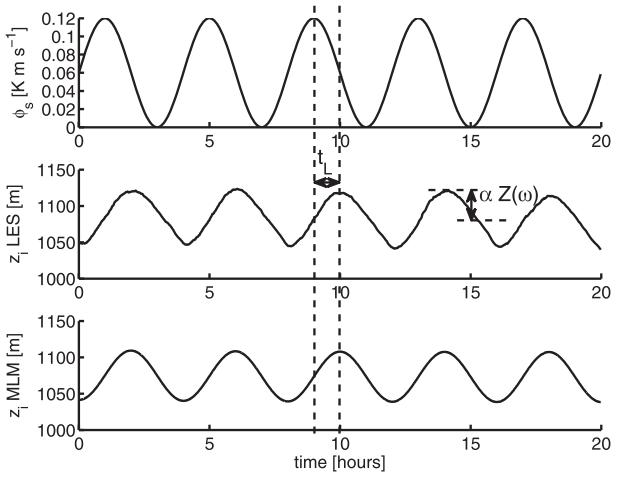

FIG. 3. (top) Example of a nonstationary surface heat flux oscillating with $T = 4$ h. (middle) Time series of the inversion height as simulated by the LES with an indication of the time lag t_L and amplitude of transfer $Z(\omega)$. (bottom) Time series of z_i as resulting from the mixed layer model (7) and (8).

averages, or phase averages for short, and are obtained by conditionally averaging the profiles based on the phase of the surface heat flux (i.e., by averaging the profiles every time when the phase of the surface heat flux has a specific value). The advantage of phase-averaged profiles over instantaneous profiles is that one can exploit the periodicity of the system and run the simulation for a very long time, covering many periods, so as to collect a large number of samples. This greatly aids the statistical quality of the averages without losing information on the nonstationary aspects of the data.

The top left graph in Fig. 4 shows the potential temperature. One can see that the inversion height and the mixed layer temperature change with the phase of the surface heat flux. The top middle graph shows the buoyancy flux; the solid gray and solid black lines correspond to the same instantaneous surface heat flux but reveal a different minimum buoyancy flux. The bottom row shows the vertical velocity variance and temperature variance, which also clearly show the time lag in the system; without history effects, the solid gray and black lines would be on top of each other.

On the basis of the heat flux profile of a constant heat flux simulation [$\phi_s(t) = \phi_0$] we have estimated the value of A, which we determined by extrapolating the linear part of the flux observed at $z < 2z_i/3$ to the inversion height z_i. A value of $A \simeq 0.34$ was found in this way and was subsequently used in the mixed layer model. This

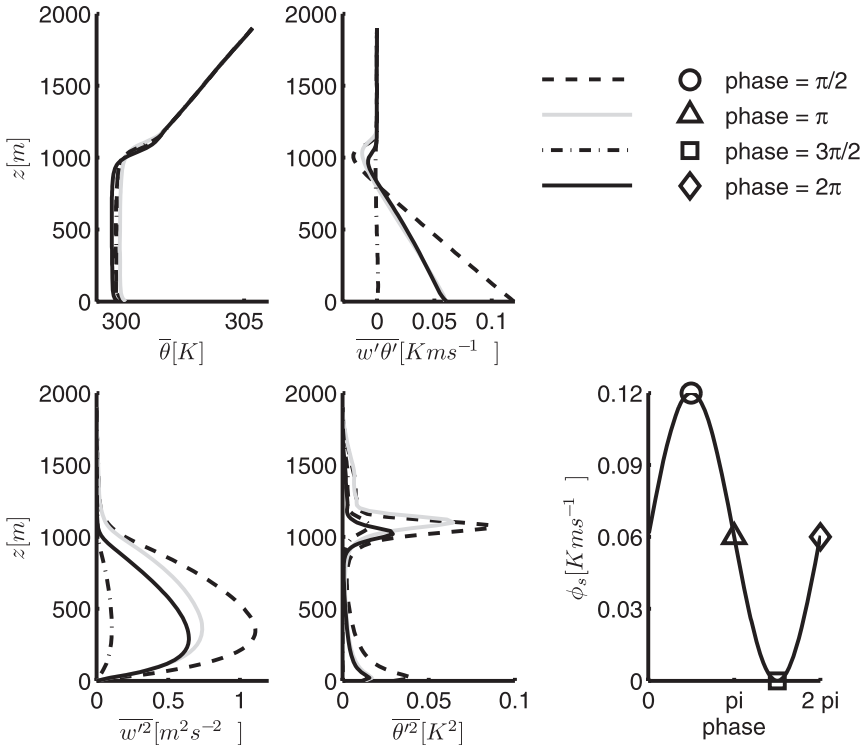

FIG. 4. Phase-conditioned averages of LES data for a nonstationary surface heat flux oscillating with $T = 4$ h. (top left) Potential temperature $\overline{\theta}$, (top middle) buoyancy flux $\overline{w'\theta'}$, variance profiles (bottom left) $\overline{w'^2}$ and (bottom middle) $\overline{\theta'^2}$, and (bottom right) the phase of the surface heat flux ϕ_s.

value for the entrainment ratio may seem somewhat high (e.g., Fedorovich et al. 2004). This is largely due to the method of extrapolating the heat flux to the inversion height, which provides values considerably bigger than the value of the minimum heat flux, in particular for weak inversions where the flux gets smeared out along the inversion zone. Another reason is that the resolution used in this study is still rather coarse. Increasing the vertical resolution to 10 m using a $256 \times 256 \times 192$ grid resulted in a decrease of A by 12% and, consistent with Eq. (9), a corresponding decrease of the inversion height by 4%. In this study, however, rather than changing the resolution, the available computing time was invested in extending the total integration time as far as possible in order to be able to simulate many oscillations of the surface heat flux. Since apart from a modest quantitative effect there appears to be no difference in the essence of the behavior between the fine and coarse resolution, all subsequent simulations are conducted on the coarse grid as reported in Table 1. Note that by setting $A = 0.34$ in the mixed layer model we effectively tune the model to the coarse-resolution LES.

The response of the mixed layer model for a nonstationary surface heat flux is shown in Fig. 3 together with the LES results. Clearly the mixed layer model is very well capable of predicting the evolution of the PBL depth for an oscillating surface heat flux. To get information on the response of the PBL for other driving frequencies $\omega = 2\pi/T$ and α, we have conducted a comprehensive study to the corresponding amplitudes $Z(\omega)$ and phase differences $\Psi(\omega)$. Results of the LES are presented in Figs. 5a and 5b together with the predictions (22) and (23) based on the linearized version of the mixed layer model. One notices that the predictions of the response work quite well for slow changes (i.e., $\omega < 10^{-4}\ \mathrm{s}^{-1}$ or T larger than approximately 17.5 h). This is interesting because the predictions appear to work well even for large α, well outside the intended working range of small amplitudes ($\alpha \ll \phi_0$). Apparently for slow changes the response of the essentially nonlinear mixed layer model (7) and (8) can be well approximated by the linearized version of the model around the stationary state (Δ_0, z_0) given by Eq. (9). Recall that this fixed point follows from the nonlinear model. A second rather striking aspect is the appreciable phase difference for small ω. Even at $\omega = 10^{-5}\ \mathrm{s}^{-1}$ ($T \simeq$ 175 h) the phase difference is about $\pi/4$, corresponding to a time lag of $t_L \approx 22$ h. Apparently the internal time scale of the boundary layer system is quite large. Mathematically this can be understood from the analysis of the eigenvalues of the system's Jacobian (14) and related time scale(s) (15) or (16), which is proportional to $2A\phi_0/(\Gamma w_s^2) \approx 10$ h. Physically this large time scale

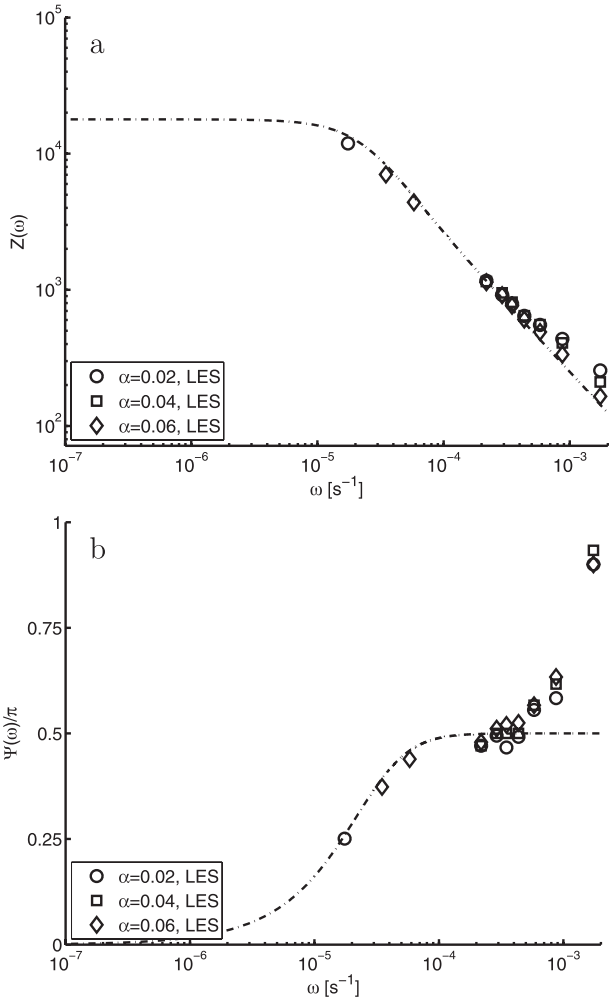

FIG. 5. Transfer function of (a) z_i amplitudes and (b) phase difference between $z_i(t)$ and $\phi_s(t)$. The analytical (linearized) solution of the standard mixed layer model (dashed lines) and the results with different amplitudes of the LES (open symbols) are shown.

can be understood by realizing that the (z_i, Δ) dynamics is governed by the entrainment velocity, leading to a time scale estimate of z_i/w_e. Steady-state considerations give $w_e = w_s$ and $z_{i0} \sim \phi_0/(\Gamma w_s)$, which leads to $t_L \sim \phi_0/(\Gamma w_s^2)$. Both w_s and Γ may differ somewhat from the values we have used here, but not much since the order of magnitude of w_s is $10^{-2}\ \mathrm{m\ s}^{-1}$, Γ is typically a few kelvins per kilometer, and surface fluxes are in the range of 0.01–0.1 K m s^{-1}. This implies that the dynamics that govern z_i and Δ are much slower than the time scale of turbulence ($\simeq$15 min) and even quite slow with respect to the time scale of the diurnal cycle itself. This in turn implies that the system will always be in a transient state, hardly adapted to the new conditions set by sunrise, sunset, or changed large-scale forcings.

Returning to Figs. 5a and 5b, one notices a discrepancy between the MLM predictions and the LES results

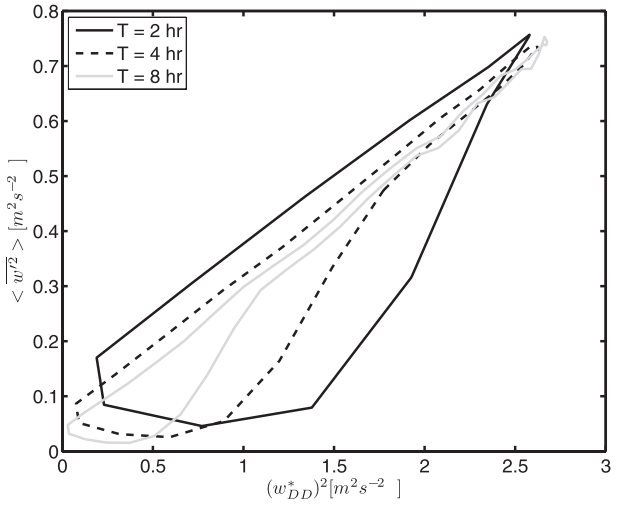

FIG. 6. Phase diagram of $\langle \overline{(w')^2} \rangle$ as obtained from the LES and the convective velocity scale (26).

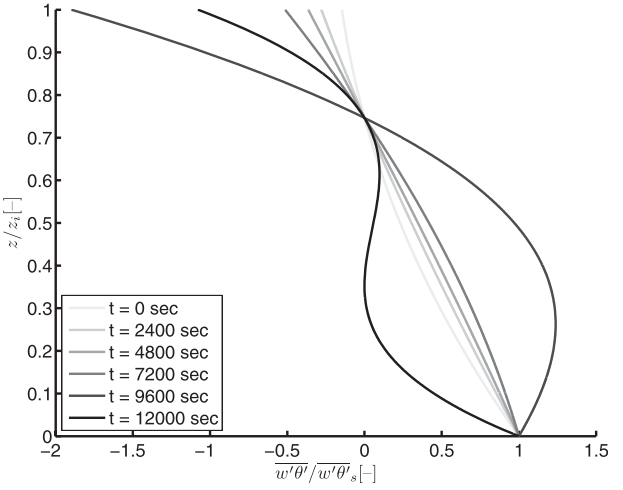

FIG. 7. Scaled $\overline{w'\theta'}$ profiles for a surface heat flux period of 4 h, following Eq. (29) with $\chi = 0.92$. The effect of the time delay produces the S-shaped curves.

for fast changes, most clearly seen at the phase differences of the LES, which are significantly larger than the maximum phase difference of $\pi/2$ resulting from the MLM. This is a natural consequence of the fact that the mixed layer model assumes instantaneous mixing, whereas in reality (and in LES) the mixing is governed by the time scales of turbulence. When the surface heat flux changes at a rate comparable to the time scale of turbulence the situation becomes more intricate. This issue is addressed in the next section.

b. *Rapidly changing surface fluxes*

For stationary surface heat fluxes the mixed layer averaged vertical velocity variance, $\langle \overline{(w')^2} \rangle$, can be well predicted (scaled) by the Deardorff (e.g., Sullivan et al. 1998) convective velocity scale:

$$w^*_{\mathrm{DD}} = \left[\frac{g z_i(t)}{\Theta_0} \phi_s(t) \right]^{1/3}. \tag{26}$$

However, for nonstationary surface heat fluxes the performance of Eq. (26) is not ideal (Sorbjan 1997). This aspect is shown in Fig. 6. When there is a good correlation (as expected for a scaling quantity), the points would lie on a line; for slowly changing fluxes ($T = 8$ h) this appears to be the case. However, for more rapidly changing fluxes the graphs obtain a circular shape indicative of the phase difference between the actual variance and the actual surface flux ϕ_s. To improve the predictions of the mixed layer model for rapidly changing surface fluxes and to come up with a better prediction of the turbulence kinetic energy levels and velocity variances, we expand the mixed layer model with an extra equation that accounts for production and dissipation (Nieuwstadt and Brost 1986):

$$\frac{\partial k(t)}{\partial t} = P(t) - C_\varepsilon \frac{k(t)^{3/2}}{z_i}, \tag{27}$$

where C_ε is a constant and where k and P represent mixed layer averages of turbulence kinetic energy and buoyancy production, respectively. The production term in this equation is modeled by

$$P(t) = \frac{1}{z_i} \int_0^{z_i} \tilde{P}(z, t)\, dz, \quad \text{with} \tag{28}$$

$$\tilde{P}(z, t) = \frac{g}{\Theta_0} \left[1 - (1 + A) \frac{z}{z_i} \right] \phi_s \left(t - \chi \frac{z}{\sqrt{k}} \right). \tag{29}$$

In this equation the essential aspect resides in the term $-\chi z/\sqrt{k}$, which accounts for the time it takes for information to travel from the surface to height z, where we have assumed that the corresponding speed scales with $\sqrt{k}$. When the turbulence kinetic energy is high, information travels fast, but when k is low it will take much longer before higher locations in the PBL can feel the changed surface properties. The constant χ can be chosen freely (once). The effect of having the time delay in Eq. (29) is that the vertical profiles of the production can depart from the (quasi-steady) linear form and potentially yield the S-shaped curves such as are observed in LES (Sorbjan 1997). The curves following from Eq. (29) at various instances are shown in Fig. 7. The constant χ in Eq. (29) was determined by comparing the production calculated by LES with the production

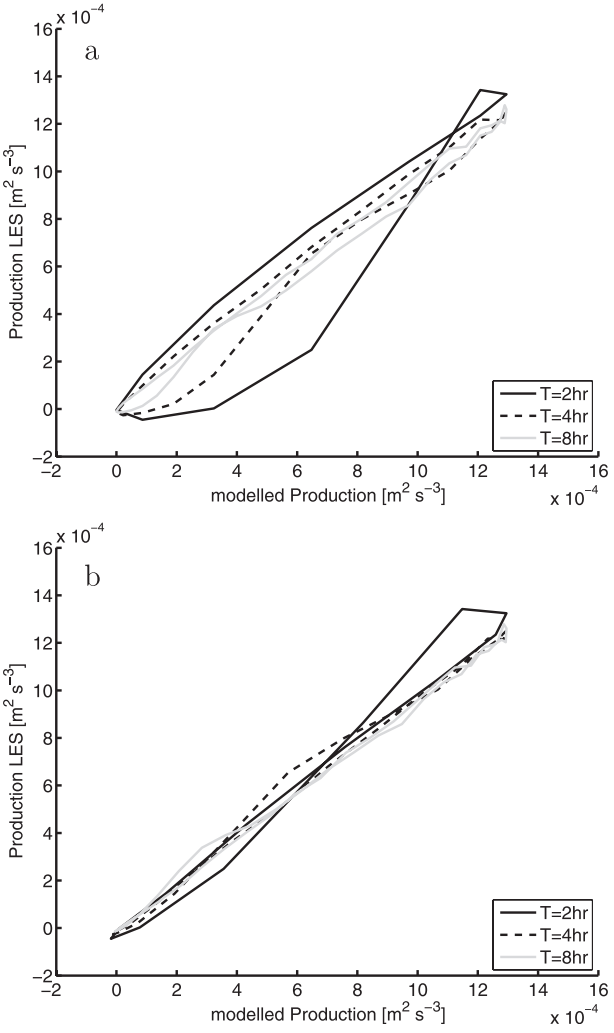

FIG. 8. The effect of χ in the production equation (29) with respect to the production of the LES results: (top) $\chi = 0$ and (bottom) $\chi = 0.92$.

calculated by Eq. (28). In this case we determined $\chi = 0.92$. The effect of having χ in Eq. (28) is shown in Fig. 8. There is a nice correlation between the results from LES and the modeled production. For periodic functions ϕ_s the integral in Eq. (28) can still be analytically solved (see appendix). Now that there is a reasonable model for the time-dependent buoyancy production, Eq. (27) can be solved once the constant C_ε has been determined. This is done by looking at the stationary state of Eq. (27), that is,

$$C_\varepsilon = \frac{P_0 z_{i0}}{k_0^{3/2}}, \tag{30}$$

where the subscript 0 refers to the stationary state of the variable. Using LES values this resulted in a value of 1.92 for C_ε. Equation (27) can now be solved, in

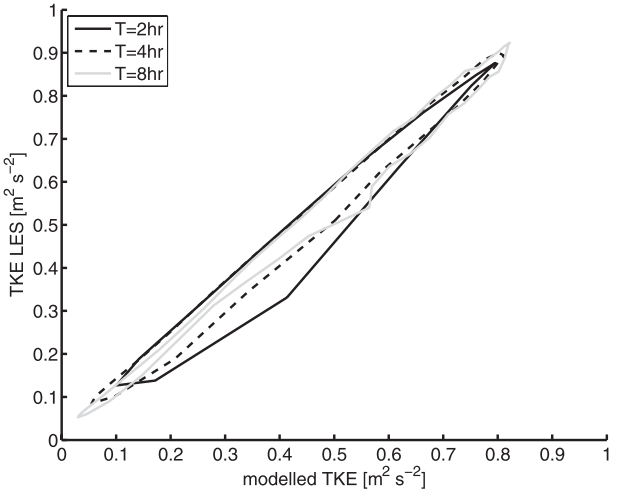

FIG. 9. TKE calculated using Eq. (27) vs TKE calculated by LES.

conjunction with the other mixed layer model equations. The result of the extended MLM is shown in Fig. 9 with respect to the turbulent kinetic energy (TKE) calculated using LES. The correlation between the LES results and Eq. (27) appears to be quite good. In Fig. 10 the result is shown with respect to the vertical velocity variance calculated using LES, which should be compared to Fig. 6. This result shows that also for rapidly changing surface fluxes the velocity variances can be anticipated while still using a simple set of equations.

Since it is possible to accurately model the turbulence kinetic energy k, we also used the prognostic value of k in the parameterization of the entrainment velocity. This parameterization starts with the usual equation for the entrainment velocity (Deardorff et al. 1980),

$$\frac{w_e}{w_*} = \frac{A}{\mathrm{Ri}}, \tag{31}$$

where Ri is the Richardson number given by

$$\mathrm{Ri} = \frac{\frac{g}{\Theta_0}\Delta z_i}{w_*^2}. \tag{32}$$

Rearranging these equations, we have for the entrainment velocity

$$w_e = \frac{A w_*^3}{\frac{g}{\Theta_0} z_i \Delta}. \tag{33}$$

The term w_*^3 represents the scaling velocity and should thus be replaced by $(\gamma k)^{3/2}$, where k is prognosticated

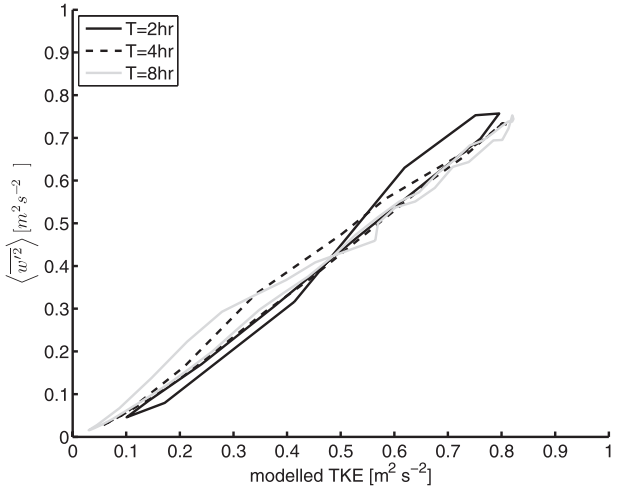

FIG. 10. TKE calculated using Eq. (27) vs $\langle \overline{(w')^2} \rangle$ determined from LES.

from Eq. (27). The constant γ can be calculated by comparing the scaling in steady state, which results in $\gamma = 3.33$.

To summarize this method, the following equations are solved in the extended mixed layer model:

$$\frac{\partial \Delta}{\partial t} = \Gamma w_e - \frac{\phi_s + \Delta w_e}{z_i}, \tag{34}$$

$$\frac{\partial z_i}{\partial t} = w_e - w_s, \tag{35}$$

$$\frac{\partial k}{\partial t} = P(t) - C_\varepsilon \frac{k^{3/2}}{z_i}, \tag{36}$$

$$P(t) = \frac{g}{\Theta_0}\frac{1}{z_i}\int_0^{z_i}\left[1 - (1+A)\frac{z}{z_i}\right]\phi_s\left(t - \chi\frac{z}{\sqrt{k}}\right)dz, \quad \text{and} \tag{37}$$

$$w_e = \frac{A(\gamma k)^{3/2}}{\frac{g}{\Theta_0} z_i \Delta}, \tag{38}$$

with constants $\chi = 0.92$, $\gamma = 3.33$, and $C_\varepsilon = 1.92$. Note that the entrainment velocity formulation (38) implies that the effective entrainment flux ratio $A_{\text{eff}} = -\phi_e/\phi_s = w_e\Delta/\phi_s$ is no longer constant. By rearranging one can recast A_{eff} into

$$A_{\text{eff}} = A\left[\frac{\gamma k(t)}{w_*^2(t)}\right]^{3/2}. \tag{39}$$

For a slowly varying heat flux $\gamma k = w_*^2$, so $A_{\text{eff}} = A$, but for a rapidly changing flux A_{eff} will deviate from A and be time dependent.

The performance of the extended MLM is shown again in terms of transfer function and phase difference. These are shown in Figs. 11a and 11b. The difference between the result of the standard MLM and the extended MLM is not so prominent in $Z(\omega)$ because the amplitudes are small anyway, but there is a marked difference in the predicted phase lag. The results of the extended MLM give comparable results to the LES result in the sense that the phase lag becomes significantly larger than $\pi/2$. The derivation of the analytical solution of the extended MLM can be found in the appendix.

Apart from sinusoidal surface fluxes, the extended MLM was put to the challenging test of a more exotic surface heat flux given by a square wave

$$\phi_s(t) = \delta + (0.12 - \delta)H\left(\frac{t}{T} \bmod 1 - \frac{1}{2}\right), \tag{40}$$

where H is the Heaviside function and T is the period of the square wave (in this case, the period is 4 h and δ is a small number; i.e., 0.001 K m s^{-1}). The sudden jumps in surface heat flux can be compared with a total solar eclipse or the modulation of the incoming solar radiation by a (dark) cloud. The results of this surface heat flux are shown in Fig. 12. Note the conspicuous bumps in the production when the heat flux increases, which are probably due to an absence of consumption by entrainment, while at the bottom there is a lot of production due to the sudden increase of the surface heat flux. On the whole, the extended MLM is again able to reproduce the turbulence kinetic energy and the production quite well. The inversion height is slightly lower than in the LES, but it is in phase and has the same amplitude as the LES results.

4. Summary and conclusions

The standard MLM works well for slowly changing surface fluxes. When the surface fluxes change with small frequencies or large periods (i.e., $\omega < 10^{-4}$ s^{-1} or $T > \sim 17.5$ h), the standard MLM gives quite good predictions. Both the transfer function and the phase difference are comparable to the LES results. However, for rapidly changing surface fluxes the standard MLM is not able to give the right predictions.

The nonlinear mixed layer model can be very well approximated by the linearized version of the model. This is remarkable because the flux perturbations are well outside the range of small amplitudes, $\alpha \ll \phi_0$, on the basis of which the linearization is carried out. Apparently the response for slow changes of the essentially nonlinear mixed layer model can be well approximated by the linearized version of the model around its stationary state, (Δ_0, z_{i0}).

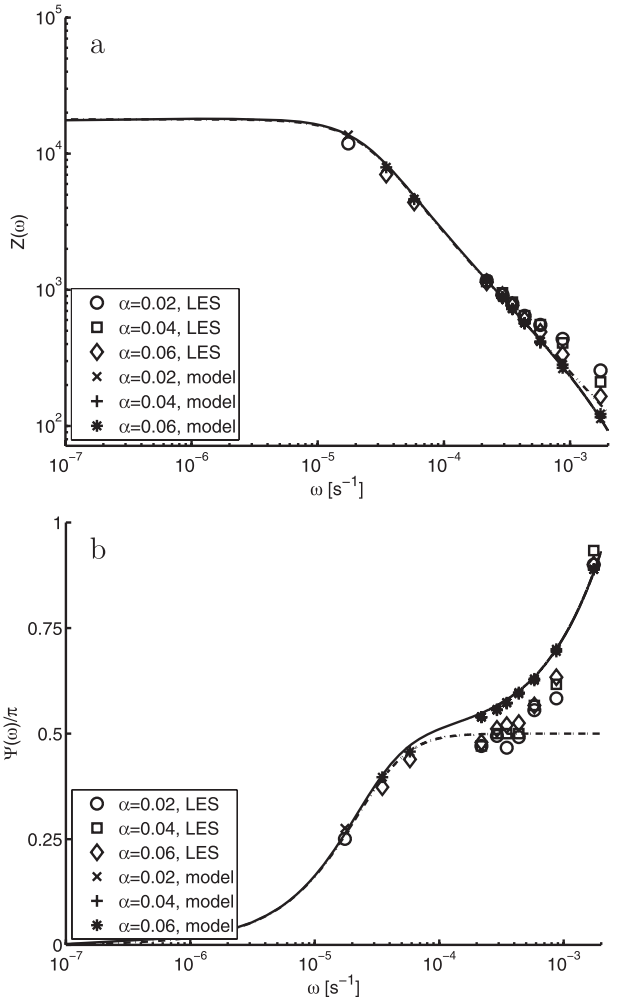

FIG. 11. Transfer function of (a) z_i amplitude and (b) the phase difference between $z_i(t)$ and $\phi_s(t)$. The analytical (linearized) solution of the extended MLM (solid lines), the results of the full (nonlinearized) new model with different amplitudes (symbols), the result of the standard MLM (dashed lines), and the results with different amplitudes of the LES (open symbols) are shown.

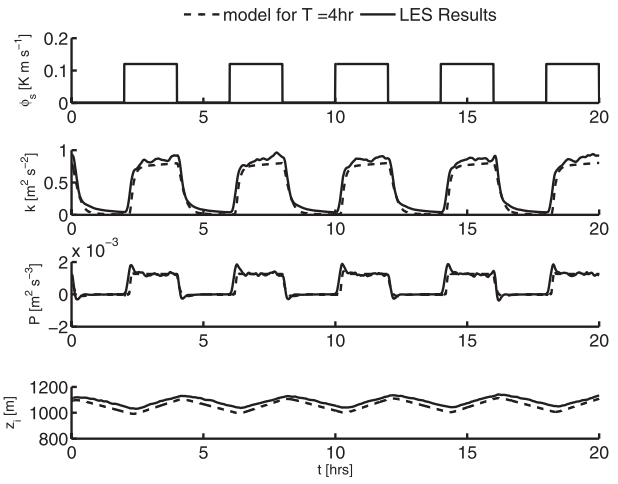

FIG. 12. Results of the extended MLM compared with the LES results for a square wave as input: (top) surface heat flux, (top middle) turbulence kinetic energy, (bottom middle) production, and (bottom) inversion height.

Very large time scales dominate the (Δ, z_i) dynamics. The time scales range from several hours until a day or more. This is surprising because usually the turbulence time scale t^* is used, which is roughly 15 min. For the phase difference between the surface heat flux and the inversion height, the time lag is even bigger. When implementing a slowly changing surface heat flux the inversion height always responds with a delay to the surface heat flux. Only for extremely slowly varying surface heat fluxes is there a vanishing phase difference.

The extended MLM performs well for both slowly and rapidly changing surface fluxes. When the standard MLM is extended with the equations for the turbulence kinetic energy and the buoyancy production the model is also able to give good predictions for rapidly changing surface fluxes. Also, the vertical velocity variances observed in LES could be scaled well using the TKE values prognosticated by the extended MLM. When changing the surface flux very fast (e.g., a square wave), the extended MLM is able to predict the turbulent kinetic energy and the production comparable to the LES results.

All in all the study shows that the behavior of a dry convective boundary layer driven by nonstationary surface heat fluxes can be understood well by invoking the relatively simple concepts of the mixed layer model and, as a consequence, that analytical solutions for the system dynamics could be derived. The problem of finding a suitable scaling relation for the vertical velocity variance during rapid changes could be dealt with by prognosticating the turbulence kinetic energy from a rate equation that comprised dissipation and buoyancy production. Also, this somewhat more involved model appears amenable to analytical study. Obviously the present study is extremely idealized and far from reality. The next step would be to include mean wind (shear) and the Coriolis force in the problem, which will change the entrainment characteristics. Finally, the stable boundary layer, as well as the transitions to and from it, should be accounted for.

Acknowledgments. This work was sponsored by the Dutch National Computing Facilities Foundation (NCF) for the use of supercomputer facilities, with financial support of NWO. The authors are grateful to Drs. Wayne

Angevine and Donald Lenschow for sharing their insight and also thank the other contributors to the BLLAST (Boundary Layer Late Afternoon and Sunset Turbulence) workshops, which were a source of inspiration for this work.

APPENDIX

Transfer Function of the Extended MLM

Without loss of generality Eq. (24) can be changed to $\phi_s = \phi_0 + \alpha \cos(\omega t)$. We can express this by $\phi_s = \phi_0 + \alpha \exp(i\omega t)$ where it is understood that in the end we are interested in the real part. The production equation as given in Eq. (37) can now be written as

$$P = \frac{g}{\Theta_0}\frac{1}{z_i}\int_0^{z_i}\left[1-(1+A)\frac{z}{z_i}\right][\phi_0 + \alpha e^{i\omega(t-\chi z/\sqrt{k})}]\,dz, \tag{A1}$$

which can be evaluated to

$$P = \frac{1-A}{2}\frac{g}{\Theta_0}\phi_0 + \alpha e^{i\omega t} g(\beta), \tag{A2}$$

where $g(\beta)$ is given by

$$g(\beta) = \frac{1}{\beta^2}[(A+1)(1-e^{-i\beta}) - i\beta(1+Ae^{-i\beta})] \tag{A3}$$

and $\beta = \beta(\omega)$ by

$$\beta(\omega) = \frac{\chi\omega z_i}{\sqrt{k}}. \tag{A4}$$

Having the expression for the buoyancy production, it is possible to apply the same method as outlined in section 2d for the plain mixed layer model, but now three equations have to be taken into account:

$$\frac{\partial \Delta}{\partial t} = \Gamma w_e - \frac{\phi_s + \Delta w_e}{z_i} = f(\Delta, z_i, k), \tag{A5}$$

$$\frac{\partial z_i}{\partial t} = w_e - w_s = g(\Delta, z_i, k), \quad \text{and} \tag{A6}$$

$$\frac{\partial k}{\partial t} = P - C_\varepsilon \frac{k^{3/2}}{z_i} = h(\Delta, z_i, k), \tag{A7}$$

where w_e is given by Eq. (38) and P is given by Eqs. (A2)–(A4). Linearization then results in

$$\frac{\partial}{\partial t}\begin{pmatrix}\Delta'\\ z_i'\\ k'\end{pmatrix} = J(\Delta_0, z_{i0}, k_0, \phi_0)\begin{pmatrix}\Delta'\\ z_i'\\ k'\end{pmatrix} + \begin{pmatrix}\frac{\partial f}{\partial \phi_s}\\ \frac{\partial g}{\partial \phi_s}\\ \frac{\partial h}{\partial \phi_s}\end{pmatrix}\phi', \tag{A8}$$

where $J(\Delta_0, z_{i0}, k_0, \phi_0)$ is the Jacobian in the fixed point. The fixed point in this case is

$$\Delta_0 = \frac{A\gamma^{3/2}\left(\frac{1-A}{2}\right)}{C_\varepsilon}\frac{\phi_0}{w_s},$$

$$z_{i0} = \left[1 + \frac{A\gamma^{3/2}\left(\frac{1-A}{2}\right)}{C_\varepsilon}\right]\frac{\phi_0}{\Gamma w_s},$$

$$k_0 = \left(\frac{z_{i0}}{C_\varepsilon}\frac{1-A}{2}\frac{g}{\Theta_0}\phi_0\right)^{2/3}. \tag{A9}$$

The driver of the system is $\phi' = \hat{\phi}\exp(i\omega t)$; Δ', z_i', and k' respond to this driver. Taking $\Delta' = \hat{\Delta}\exp(i\omega t)$, $z_i' = \hat{z}_i \exp(i\omega t)$, and $k' = \hat{k}\exp(i\omega t)$, the system (A8) becomes

$$i\omega\begin{pmatrix}\hat{\Delta}\\ \hat{z}_i\\ \hat{k}\end{pmatrix} = J(\Delta_0, z_{i0}, k_0, \phi_0)\begin{pmatrix}\hat{\Delta}\\ \hat{z}_i\\ \hat{k}\end{pmatrix} + \begin{pmatrix}\frac{\partial f}{\partial \phi_s}\\ \frac{\partial g}{\partial \phi_s}\\ \frac{\partial h}{\partial \phi_s}\end{pmatrix}\hat{\phi}. \tag{A10}$$

This can be written as

$$\begin{pmatrix}\hat{\Delta}\\ \hat{z}_i\\ \hat{k}\end{pmatrix} = [i\omega\mathbf{I} - J(\Delta_0, z_{i0}, k_0, \phi_0)]^{-1}\begin{pmatrix}\frac{\partial f}{\partial \phi_s}\\ \frac{\partial g}{\partial \phi_s}\\ \frac{\partial h}{\partial \phi_s}\end{pmatrix}\hat{\phi}, \tag{A11}$$

where $\mathbf{I}$ is the unit matrix. Solving Eq. (A11) gives an expression for $\hat{z}_i$, among others.

REFERENCES

Acevedo, O. C., and D. R. Fitzjarrald, 2001: The early evening surface-layer transition: Temporal and spatial variability. *J. Atmos. Sci.,* **58,** 2650–2667.

Anfossi, D., G. Schayes, G. De Grazia, and A. Goulart, 2004: Atmospheric turbulence decay during the solar total eclipse of 11 August 1999. *Bound.-Layer Meteor.,* **111,** 301–311.

Angevine, W. M., H. Klein Baltink, and F. C. Bosveld, 2001: Observations of the morning transition of the convective boundary layer. *Bound.-Layer Meteor.,* **101,** 209–227.

Ball, F. K., 1960: Control of inversion height by surface heating. *Quart. J. Roy. Meteor. Soc.,* **86,** 483–494.

Beare, R. J., 2008: The role of shear in the morning transition boundary layer. *Bound.-Layer Meteor.,* **129,** 395–410.

——, J. M. Edwards, and A. J. Lapworth, 2006: Simulation of the observed evening transition and nocturnal boundary layers: Large-eddy simulation. *Quart. J. Roy. Meteor. Soc.,* **132,** 81–99.

Deardorff, J. W., G. E. Willis, and B. H. Stockton, 1980: Laboratory studies of the entrainment zone of a convectively mixed layer. *J. Fluid Mech.,* **100,** 41–64.

Dolas, P. M., R. Ramchandran, K. Sen Gupta, S. M. Patil, and P. N. Jadhav, 2002: Atmospheric surface-layer processes during the total solar eclipse of 11 August 1999. *Bound.-Layer Meteor.,* **104,** 445–461.

Fedorovich, E., R. Conzemius, and D. Mironov, 2004: Convective entrainment into a shear-free, linearly stratified atmosphere: Bulk models reevaluated through large-eddy simulations. *J. Atmos. Sci.,* **61,** 281–295.

Girard-Ardhuin, F., B. Bénech, B. Campistron, J. Dessens, and S. Jacoby-Koaly, 2003: Remote sensing and surface observations of the response of the atmospheric boundary layer to a solar eclipse. *Bound.-Layer Meteor.,* **106,** 93–115.

Goulart, A., G. Degrazia, U. Rizza, and D. Anfossi, 2003: A theoretical model for the study of convective turbulence decay and comparison with large-eddy simulation data. *Bound.-Layer Meteor.,* **107,** 143–155.

Grant, A. L. M., 1997: An observational study of the evening transition boundary-layer. *Quart. J. Roy. Meteor. Soc.,* **123,** 657–677.

Heus, T., and Coauthors, 2010: Formulation of and numerical studies with the Dutch Atmospheric Large-Eddy Simulation (DALES). *Geosci. Model Dev. Discuss.,* **3,** 99–180.

Jonker, H. J. J., P. G. Duynkerke, and J. W. M. Cuijpers, 1999: Mesoscale fluctuations in scalars generated by boundary layer convection. *J. Atmos. Sci.,* **56,** 801–808.

Kumar, V., J. Keissl, C. Meneveau, and M. B. Parlange, 2006: Large-eddy simulation of a diurnal cycle of the atmospheric boundary layer: Atmospheric stability and scaling issues. *Water Resour. Res.,* **42,** W06D09, doi:10.1029/2005WR004651.

Lapworth, A., 2003: Factors determining the decrease in surface wind speed following the evening transition. *Quart. J. Roy. Meteor. Soc.,* **129,** 1945–1968.

——, 2006: The morning transition of the nocturnal boundary layer. *Bound.-Layer Meteor.,* **119,** 501–526.

Lilly, D. K., 1968: Models of cloud-topped mixed layers under a strong inversion. *Quart. J. Roy. Meteor. Soc.,* **94,** 292–309.

Mahrt, L., 1981: The early evening boundary layer transition. *Quart. J. Roy. Meteor. Soc.,* **107,** 329–343.

Nieuwstadt, F. T. M., and R. A. Brost, 1986: The decay of convective turbulence. *J. Atmos. Sci.,* **43,** 532–546.

Pino, D., H. J. J. Jonker, J. Vilà-Guerau de Arellano, and A. Dosio, 2006: Role of shear and the inversion strength during sunset turbulence over land: Characteristic length scale. *Bound.-Layer Meteor.,* **121,** 537–556.

——, and Coauthors, 2010: Studying the Boundary Layer Late Afternoon and Sunset Turbulence (BLLAST). *Extended Abstracts, 19th Symp. on Boundary Layer Turbulence,* Keystone, Colorado, Amer. Meteor. Soc., P1.1. [Available online at http://ams.confex.com/ams/19Ag19BLT9Urban/techprogram/paper_172180.htm.]

Sorbjan, Z., 1997: Decay of convective turbulence revisited. *Bound.-Layer Meteor.,* **82,** 501–515.

——, 2007: A numerical study of daily transitions in the convective boundary layer. *Bound.-Layer Meteor.,* **123,** 365–383.

Sullivan, P. P., C.-H. Moeng, B. Stevens, D. Lenschow, and S. D. Mayor, 1998: Structure of the entrainment zone capping the convective atmospheric boundary layer. *J. Atmos. Sci.,* **55,** 3042–3064.

Tennekes, H., 1973: A model for the dynamics of the inversion above a convective boundary layer. *J. Atmos. Sci.,* **30,** 558–567.

Vilà-Guerau de Arellano, J., B. Gioli, F. Miglietta, H. J. J. Jonker, H. K. Baltink, R. W. A. Hutjes, and A. A. M. Holtslag, 2004: Entrainment process of carbon dioxide in the atmospheric boundary layer. *J. Geophys. Res.,* **109,** D18110, doi:10.1029/2004JD004725.